doi: 10.1016/j.jmbbm.2020.104142.

Nickel-Titanium peripheral stents: which is the best criterion for the multi-axial fatigue strength assessment?

Francesca Berti[1,2], Pei-Jiang Wang[2], Andrea Spagnoli[3], Giancarlo Pennati[1], Francesco Migliavacca[1], Elazer R Edelman[2], Lorenza Petrini[4*]

[1]Laboratory of Biological Structure Mechanics, Department of Chemistry, Materials and Chemical Engineering "Giulio Natta", Politecnico di Milano, Piazza Leonardo da Vinci 32, 20133 Milano (Italy)
[2]Biomedical Engineering Center, Institute for Medical Engineering & Science, Massachusetts Institute of Technology, Cambridge, MA, USA
[3]Department of Engineering and Architecture, Università di Parma, Parco Area delle Scienze, 181/A - 43124 Parma (Italy)
[4]Department of Civil and Environmental Engineering, Politecnico di Milano, Piazza Leonardo da Vinci 32, 20133 Milano (Italy)

Keywords: multi-axial fatigue; shape-memory device; peripheral stent; Ni-Ti; fatigue criterion

*Corresponding authors.
Tel.: +39 02 2399 4307
fax: +39 02 2399 4286.
E-mail address: lorenza.petrini@polimi.it

Conflict of interest

The authors declare no conflict of interest.

Authors contribution

Francesca Berti: investigation, visualization, methodology, software, formal analysis, writing – original draft, writing – review & editing

Pei-Jiang Wang: formal analysis, writing – review & editing

Andrea Spagnoli: conceptualization, methodology, writing – review & editing

Giancarlo Pennati: conceptualization, methodology

Francesco Migliavacca: supervision, visualization, writing – review & editing

Elazer R Edelman: supervision, resources, supervision, writing – review & editing

Lorenza Petrini: supervision, conceptualization, investigation, methodology, visualization, writing – review & editing

Highlights

1) Ni-Ti stents are subjected to multiple loads in the physiological environment which affects their fatigue life
2) The local stress/strain response is strongly non-proportional regardless of the nature of the remote load
3) The common fatigue approach based on the von Mises yield criterion leads to an underestimation of the probability of failure
4) The Brown-Miller and Smith-Watson-Topper critical-plane based approaches allow more realistic interpretation of fatigue failure

E_M	the elastic modulus for the martensite phase	k, S	empirical material constant accounting for the coupling of shear/bending fatigue strength at 10^6 cycles
E_A	the elastic modulus for the austenite phase	σ_y	material monotonic yield strength
ν	Poisson's ratio	σ_{max}	maximum normal stress
ε_L	the amplitude of the transformation plateaus	$\sigma_{n,max}$	maximum normal stress on the critical plane
$\frac{\Delta\varepsilon_1}{2}$	first principal strain amplitude	σ_{SSA}	starting stress value for the reverse phase transformation
$\frac{\Delta\varepsilon_2}{2}$	second principal strain amplitude	σ_{SAS}	starting stress value for the forward phase transformation
$\frac{\Delta\varepsilon_3}{2}$	third principal strain amplitude	σ_{FSA}	final stress value for the reverse phase transformation
$\frac{\Delta\varepsilon_n}{2}$	normal strain amplitude on the critical plane	σ_{FAS}	final stress value for the forward phase transformation
$\frac{\Delta\gamma_{max}}{2}$	maximum shear strain amplitude on the critical plane	σ_{SAS}^{C}	starting stress value for the forward phase transformation in compression
$\frac{\Delta\varepsilon_{max}}{2}$	maximum normal strain amplitude on the critical plane		

Abstract

Ni-Ti stents fatigue strength assessment requires a multi-factorial complex integration of applied loads, material and design and is of increasing interest. In this work, a coupled experimental-numerical method for the multi-axial fatigue strength assessment is proposed and verified for two different stent geometries that resemble commercial products. Particular attention was paid to the identification of the material fatigue limit curve. The common approach for the Ni-Ti stents fatigue assessment based on the von Mises yield criterion was proven unsuitable for a realistic fatigue strength assessment. On the other hand, critical plane-based criteria were more representative of the experimental outcomes regardless of stent design.

1. Introduction

Nickel-Titanium (Ni-Ti) is a shape memory alloy widely used in biomedical fields. Its temperature-dependent pseudo-elasticity allows design of self-expandable devices for mini-invasive deployments e.g. stents for the treatments of peripheral occlusive diseases (Duerig et al., 1999; Petrini and Migliavacca, 2011). Though so strong that the material was used in the nose cones of missiles, fatigue failure in Ni-Ti peripheral stents remains a multi-factorial open issue due to: i) the complexity of the applied loads, ii) the non-linear material characteristic curve and iii) the design procedure.

Peripheral stents are crimped onto a delivery catheter which allows in-situ deployment into an atherosclerosed vessel; their diameter is reduced up to about 1 mm and maintained in such configuration until release which triggers a pseudo-elastic response that restores the original dimension. Stents come in a large variety of length/diameter combinations. Typically, the implantation occurs with 1 mm oversizing: it means that, for example, a 6 mm nominal outer diameter is implanted into a 5 mm vessel to ensure just the right amount of radial force to keep the vessel open without subsequent injury. This overzing induces mean strain in the v-struts elements of the stent. When implanted in peripheral vessels interaction with by muscle and ligaments with low extremity motion produces a complex cyclic set of non-proportional axial compression, bending and torsion that is transmitted through the peripheral vessels into the stents (Ansari et al., 2013).
The Ni-Ti stress-strain curve exhibits a flag-shaped morphology, with a wide stress plateau, allowing a strain-based focus for durability assessment. The material behavior is strongly affected by the thermo-mechanical treatment during manufacturing. Peripheral stents are usually laser-cut from a source tube (about 2 mm in diameter) – subsequent shape-setting (multiple heatings and quenchings) produces the definitive expanded configuration and desired mechanical properties. A final surface finishing, such as electro-polishing, reduces defect propagation to fatigue crack formation. Robertson et al. (Robertson et al., 2012) studied Ni-Ti fatigue behavior, highlighting how fatigue cracks in Ni-Ti specimens, such as stents with v-struts about 0.2 mm thick, quickly lead to the failure of the component. Few studies have analyzed fracture modes in these small parts as it is difficult to properly identify nucleation and propagation phases.

Ni-Ti fatigue characterization is usually performed through uniaxial tensile tests on ad-hoc specimens, investigating different levels of strain mean value and amplitude. The results of these tests are commonly reported in a “strain-life diagram”, where strain amplitude is plotted against the number of cycles to failure (under fixed mean value), or in a “constant-life diagram”, which examines strain amplitude versus mean strain (at fixed number of cycles to failure). The latter more efficiently verifies the effect of the mean strain (that could be related to the radial oversizing of the stent after the in-vivo deployment into the artery) on the fatigue behavior. Such an effect is rather distinctive of Ni-Ti, which, conversely to conventional metal materials like stainless steel or chromium-cobalt alloys, exhibits an increase in the fatigue limit with increasing mean strain (Pelton et al., 2008).

Though companies manufacturing peripheral stents commonly use their own design rules, combining different arrangements of rings, v-struts and connecting links, a common feature can be recognized in the bending-dominated deformation mode of the v-struts, in which high gradients arise. To fulfill certification requirements, the stents are designed to survive a minimum required number of loading cycles, which could be up to 10^8 for cardiovascular applications, while it is limited to 10^7 for peripheral stents (ASTM, 2013; Kinkel et al., 2009). A common design method is the so-called “testing for survival”, where several devices are experimentally verified under in-vivo like boundary conditions. This is an effective but expensive method that consumes large sums and time, and can consider relatively few testing conditions. According to FDA (Food and Drug Administration) guidelines (Morrison, 2016), numerical tools like the finite element (FE) method represents an effective strategy to analyze all these aspects, since the disadvantages (high costs, long duration, difficulty in reproducing the in vivo environment, impossibility to measure in-situ biomechanical values) of performing

several experimental tests can be avoided (Dordoni et al., 2015).

To fully exploit the potential of FE tools, local 3D strain fields in the device have to be compared to a reference strain threshold related to the material fatigue limit [5]. Many multi-axial fatigue criteria have been proposed and experimentally verified for standard metals, considering different materials and, hence, failure modes. However, no specific criteria have been developed for Ni-Ti alloys. In particular, the common practice for Ni-Ti stents fatigue assessment is based on the transformation of a fully tridimensional state of strain/stress in an equivalent scalar quantity in order to allow the comparison with the fatigue material limit obtained through uniaxial tests. One of the most frequently used quantity is the strain amplitude calculated according to the definition of the von Mises equivalent strain, which suggested to improperly define this approach as "von Mises fatigue criterion"(Mahtabi and Shamsaei, 2015; Runciman et al., 2011). Also in the following, for the sake of simplicity, we will use the same terminology, well aware of the not correctness of the term. In any case, the use of the von Mises equivalent or first principal strain amplitude for multi-axial fatigue assessment is not supported by experimental proof of sufficient reliability, so that other criteria, based on the concept of the critical plane, have recently been proposed to better account for multi-axial and non-proportional loads (Suresh, 1998; Susmel, 2009).
To fully assess the prediction capability of a multi-axial fatigue criterion in the Ni-Ti stents assessment, an experimental campaign together with a detailed comparison with the results obtained through FE models is presented in this paper.
Thanks to the results obtained from a previous investigation (Berti et al., 2019), in which it has been demonstrated that even if the remote applied load is uniaxial or multi-axial but proportional, the local strain response is highly non-proportional, this paper focuses on multi-axial criteria based on the critical plane approach.

Two different stent designs resembling commercial units were manufactured and analyzed in this study. These belong to the same manufacturing batch of those employed in previous research of the authors (Allegretti et al., 2018), where the Ni-Ti stent fatigue behavior under uniaxial tension only loads was investigated. In this work, multi-axial tests mimicking in-vivo conditions are performed under different load magnitudes, to increase the knowledge in the multi-axial fatigue strength assessment of these Ni-Ti stents. Corresponding FE simulations, mimicking all the experiments, were carried out and the stress/strain outputs were combined according to four criteria (Von Mises, Fatemi-Socie, Brown-Miller, and Smith-Watson-Topper, which represent the up-to-date most common literature choices as reviewed in (Berti et al., 2019)). Comparing the numerical results with the material fatigue limit, experimentally identified for the specific material of the stent, allowed us to verify which criterion was able to predict the in vitro fatigue data.

2. Materials and methods

2.1 Experimental tests and FE modeling

Two different stent designs resembling the commercial Absolute Pro® (Abbott Vascular, Santa Clara, CA) and Complete® SE (Medtronic Vascular, Santa Rosa, CA) peripheral vascular stents were laser-cut from a source tube (inner and outer diameters of 1.7 and 2.18 mm, respectively) (Figure 1 a,b). Then, they underwent first chemical etching and mechanical deburring, followed by shape setting combined with repeated heat treatments. This phase guaranteed a stress-free final configuration of the device, exploiting pseudo-elasticity at body temperature (37°C). Sand blasting and electro-polishing were performed on all the samples to remove defects due to the laser-cutting.

The considered portion of the stent Absolute Pro® (in the following ABS) is composed of 3 rings connecting peak-to-valley by straight links: the total longitudinal length is about 9 mm and the rings are composed of struts ~ 2 mm in length, 200 μm thick and 100 μm wide, in a v-shaped assembly (Figure 1a). The stent Complete® SE (in the following COMP) is composed of 4 rings of 8 mm length, connecting peak-to-peak by small links (Figure 1b). The v-struts are of the same dimensions of the previous stent and for both the stents the inner diameter in the expanded configuration is 6 mm.

Ad-hoc multi-wires specimens (with three parallel wires, Figure 1 c) were laser-cut from the same tube and underwent the same thermal treatments and surface finishing of the stents to ensure similar material and mechanical properties. Each wire gauge length was 15 mm and the cross-section of 0.25 mm, compatible with that of the v-struts. These specimens allowed the static and fatigue characterization of the specific material. Samples were visually and geometrically inspected/measured prior to fatigue testing. Three static tests were performed according to ASTM F2516-18 (ASTM F 2516-18, 2018), consisting of uniaxial tensile tests up to 6% nominal strain, followed by unloading, and then reloading up to 9%; the range of material permanent plastic strains was not investigated, resulting negligible in this kind of applications. The load-displacement curve was translated into the true stress-strain one according to the geometry of the sample. For the fatigue tests, two samples were cyclically tested at 1 Hz at different levels of mean strain and strain amplitude (meaning 6 Ni-Ti wires tested at each load level), to investigate the loads typical for stents (between 1 and 8% mean strain, up to 1% amplitude). The static tests were used to calibrate the corresponding material parameters through the multi-wire FE model, while the fatigue data were used to deduce the material fatigue limit curve at 10^6 cycles. The choice of this threshold is justified by the fact that Ni-Ti has an almost constant fatigue behavior after 10^5 cycles (Pelton et al., 2008). Note that the conversion between applied displacements and mean/amplitude strain levels can be directly achieved from the imposed boundary conditions of the experiments, given the simple geometry of the wire.

Experimental fatigue tests on the stents were carried out to reproduce in-vivo boundary conditions and, hence, stent fracture. Then, a customized fixture, which was adapted to reside within the dynamic testing system Instron ElectroPuls E1000 (Norwood, MA), converted machine axial motion into multi-axial proportional loads, namely axial compression (A), bending (B), and torsion (T), acting on the stent (Figure 2 a). The machine was equipped with a highspeed camera that allowed us to verify the applied displacements and rotations. The environment was temperature-controlled at 37.0±0.1° C to guarantee the pseudo-elastic properties of the stents. Preliminary tests allowed us to guarantee a stable temperature of the tested sample. Each stent was inserted into the testing system and left still for about 1 hour before the test, to guarantee the environmental temperature to stabilize. The sensor connected to the retroactive heating element was positioned about 2 cm apart from the stent. Also, a thermocouple was inserted into the chamber to check the local temperature of the stent struts, which was compatible with that recorded by the heating system.
As previously mentioned, the crimping and implantation phases are responsible for a state of non-zero mean stress/strain that influences the following cyclic deformations induced by vascular and lower-limb motion. In

our experimental campaign, both stent geometries were tested in their expanded configuration with a preload inducing a stress/strain state resembling a realistic implantation scenario. Each stent was constrained to 3D-printed ad hoc supports, which allowed an automatic alignment with the machine actuators when inserted into the testing system. This was considered the initial condition of the test when the stent was in its stress-free configuration. Then, a preload was applied, consisting of an in-phase application of A, B, T loads properly calibrated to introduce a local strain field representative of the crimping procedure. Then, the stent was partially released, to mimic the expansion into the vessel taking into account oversizing. The fatigue test started with the pulsation from this configuration.
All the high-cycle fatigue investigations were performed at 1 Hz, mimicking the frequency of gait. This choice limited the possibility to perform an extensive campaign up to millions of cycles, and the experimental run-out was set at 10^6 cycles. Three different cyclic load levels, namely P1, P2 and P3 were investigated, having fatigue ratio (minimum load divided by the maximum load) R=0.75, 0.62 and 0.71 respectively (Figure 2 c). The loading condition P1 can be considered representative of the physiological boundary conditions acting on a peripheral stent when implanted in the lower limbs. The choice of P2 and P3 came directly by the need of obtaining different outputs from the chosen fatigue criteria, losing a direct correspondence with the in-vivo loads. More details regarding the boundary conditions are shown in Table 1.

All the simulations were performed in the Abaqus 2018/Standard environment (Dassault Systemes, SIMULIA Corp., RI). The constitutive model available in Abaqus for super-elastic material was used. The required parameters, namely the Young's moduli of the austenite and martensite (E_A and E_M), the amplitude of the transformation plateaus (ε_L), the four stress values, defining the start and finish of the forward ($A \rightarrow S$) and the reverse ($S \rightarrow A$) transformations (σ_{SAS}, σ_{FAS}, σ_{SSA}, σ_{FSA}) in tension were calibrated from the experiments on the multi-wires specimens while the forward transformation starting stress in compression (σ^c_{SAS}, due to the material asymmetry), was taken from (Allegretti et al., 2018). The value of the Poisson's ratio (ν) was taken from the literature (Maletta et al., 2016; Scalet et al., 2017). More information regarding the model validation can be found in (Allegretti et al., 2018). The multi-wires FE model was used both for the material calibration and for obtaining the tensile stress/strain in the gauge length associated with each fatigue load level. The FE models of the stents were available from previously published work of the authors [11], where the fatigue behavior of ABS and COMP under axial loading was investigated. Details regarding the models' geometry and discretization are available in (Allegretti et al., 2018; Berti et al., 2019).

The ABS and COMP models were meshed using 196890 and 203320 8-nodes solid elements with incompatible mode formulation (comparable element type according to ANSYS SOLID185 with enhanced strain formulations), respectively, according to the sensitivity analysis performed in (Allegretti et al., 2018). Different mesh refinements were compared in terms of first principal stress and strain at the maximal loaded points of the structures and global reaction force when the model was axially tensioned. The optimal mesh density was a compromise between computational cost and result accuracy.

Previous FE analysis (Petrini et al., 2016) demonstrated that the mean strain value at the end of the stent deployment in the vessel was strictly location-dependent around the stent, but nowhere it overcame 5%. In our numerical simulations, as in the experiments, the stents were analyzed in their expanded configuration following the preload phase discussed above. Then, the same proportional combinations of axial compression (A), bending (B), and torsion (T) loads chosen for the experiments (Table 1) were applied through two Multi-Point-Constraints (MPCs) to both the stents (Figure 2 b).

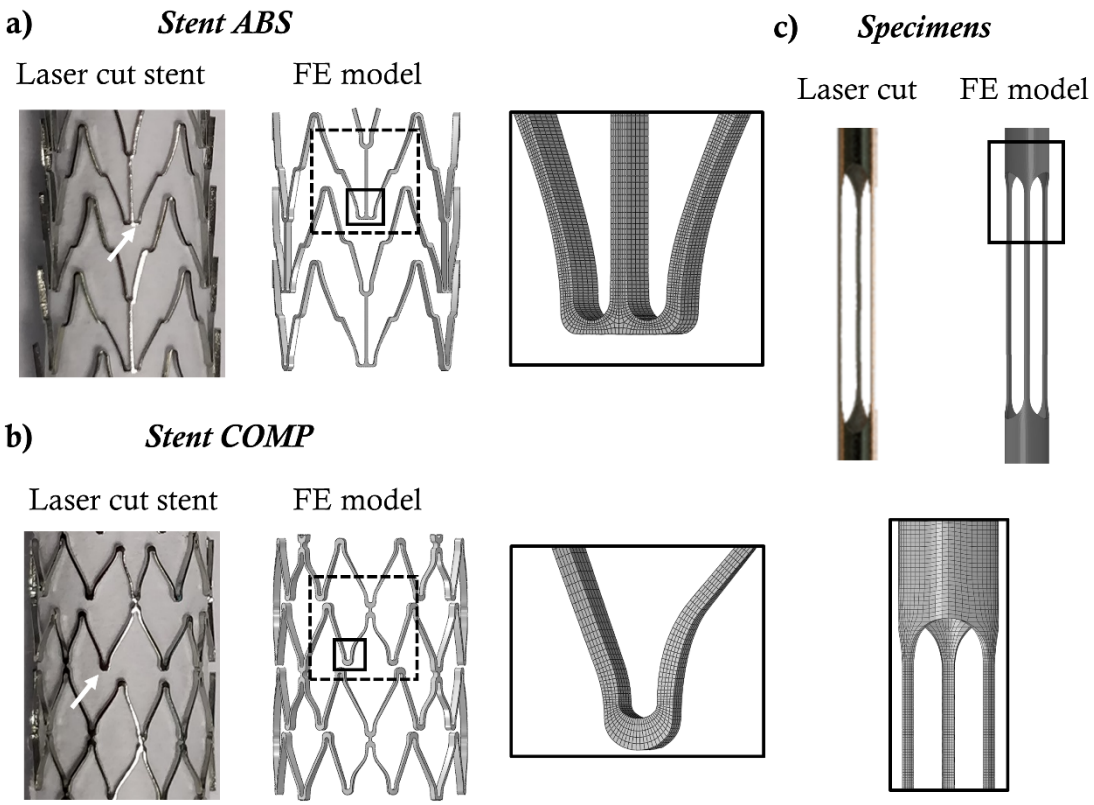

Figure 1 a) Comparison of the laser cut stent ABS and its FE model, with a detail of the mesh; b) comparison of the laser cut stent COMP and its FE model, with a detail of the mesh; white arrows indicated the area where the failure occurred; c) ad-hoc developed multi-wire specimen and the associated FE model with a detail of the mesh. Dashed boxes indicate the two functional units.

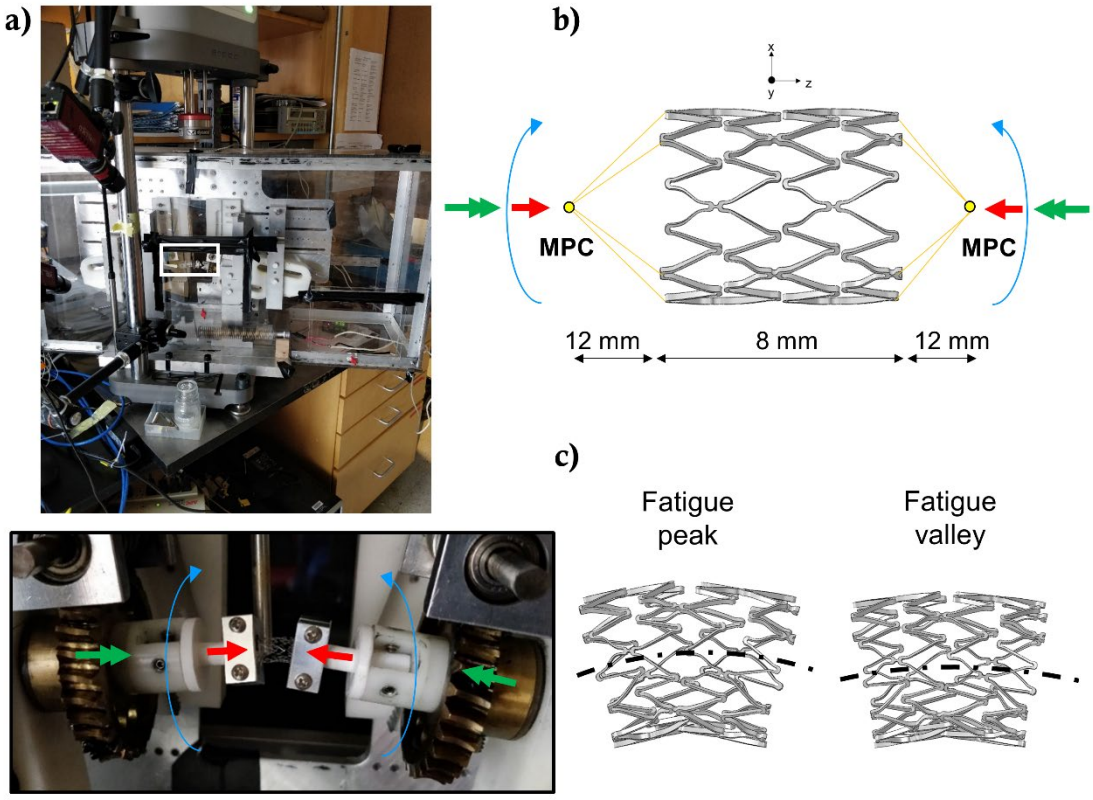

Figure 2 a) The experimental set-up for multi-axial loading with an insight of the boundary conditions; b) the combined load applied to the COMP stent, through the MPCs constraints: the red arrow indicates the axial compression (A), the blue arrow the bending (B) and the green arrow the torsion (T); c) deformed configuration of COMP stent under P1 combination at the reversals of the fatigue cycle. The MPCs are located 12 mm away from the stent ends to be representative of the machine clamps.

Table 1 Different loading combinations with in-phase axial compression (A), bending (B) and torsional (T) actions. Case P1 resembles a physiologically-like deformation pattern during walking (Ansari et al., 2013; MacTaggart et al., 2014). The number of stents tested in-vitro in each configuration is also reported according to the different designs.*These boundary conditions, which are the same for both stent ABS and COMP, are applied symmetrically at the MPCs.

Loads	A, B, T *						In-vitro tests	
	ΔA		ΔB		ΔT		ABS	COMP
	peak	valley	peak	valley	peak	valley		
P1 (R=0.75)	1.26 mm	0.93 mm	30°	23°	30°	23°	2	2
P2 (R=0.62)	1.50 mm	0.93 mm	36°	23°	36°	23°	3	3
P3 (R=0.71)	1.31 mm	0.93 mm	32°	23°	32°	23°	3	2

2.2 Multi-axial fatigue strength criteria

A multi-axial fatigue criterion is needed to convert the 3D information of the stress/strain tensors in the stents into a uniaxial effective quantity. The same four different fatigue criteria investigated in (Allegretti et al., 2018; Berti et al., 2019) were considered to compute a fatigue index (FI). Since they are based on different mechanical assumptions, the comparison of their output can give an insight into their capability of interpreting the stents' failure happening under in-vivo-like loads. The von Mises (VM) index, identified as the equivalent alternate strain, was calculated by using strain tensors extracted from the two time increments corresponding to the peak and valley of the fatigue cycle. The difference between the two tensors was calculated for obtaining the alternate strain tensor, from which the alternate values of the principal strains were derived, namely $\Delta\varepsilon_1$, $\Delta\varepsilon_2$, $\Delta\varepsilon_3$ (Eq.1). The Fatemi-Socie (FS) (Fatemi and Socie, 1988) is a strain-based critical plane criterion for shear failure mode materials, which is a function of both the maximum shear strain amplitude ($\Delta\gamma_{max}/2$) and the maximum value of normal stress ($\sigma_{n,max}$), both acting on the plane of the maximum shear strain amplitude (Eq. 2). The herein reported fatigue parameter G $\Delta\gamma$ ($\Delta\gamma$ is the shear strain range on the maximum shear strain plane) is recently proposed in (Gates and Fatemi, 2016) to replace the yield strength. This new version of FS criterion results in improved fatigue life correlations in the presence of mean stress, even though it maintains all the advantages and physical interpretations of the original criterion (Shahriar and Fatemi, 2019). The Brown-Miller (BM) (Brown and Miller, 1973) is also a strain-based criterion which combines the maximum shear strain amplitude and the maximum normal strain amplitude ($\Delta\varepsilon_n/2$) that occurs in a cycle on the plane experiencing the maximum shear strain amplitude (Eq.3). The Smith-Watson-Topper (SWT) (Smith, K.N., Topper, T.H., Watson, 1970; Socie, 1987) is an energy-based approach and the FI is given by the product of the maximum normal stress and the maximum normal strain amplitude, both on the plane of maximum normal strain (Eq.4).

$$VM = \frac{1}{2(1+\nu)\sqrt{2}}\sqrt{(\Delta\varepsilon_1 - \Delta\varepsilon_2)^2 + (\Delta\varepsilon_2 - \Delta\varepsilon_3)^2 + (\Delta\varepsilon_3 - \Delta\varepsilon_1)^2} \quad (1)$$

$$FS = \frac{\Delta\gamma_{max}}{2}\left(1 + k\frac{\sigma_{n,max}}{G\,\Delta\gamma}\right) \quad (2)$$

$$BM = \frac{\Delta\gamma_{max}}{2} + S\frac{\Delta\varepsilon_n}{2} \quad (3)$$

$$SWT = \sigma_{n,max}\,\frac{\Delta\varepsilon_n}{2} \quad (4)$$

The empirical constants k and S, employed in the FS and BM criteria, were taken as equal to 1 as suggested in (Shamsaei and Fatemi, 2009; Socie et al., 1985).

In (Allegretti et al., 2018), the computation of the FIs according to each criterion was performed considering the values of the stress and strain tensors at the maximum and minimum values of the fatigue cycle. The current paper improved this aspect by discretizing the cycle in many time instants and by performing the calculation

of the critical plane-related stress/strain quantities according to the work of Papadopoulos (1998). This guarantees a higher accuracy when dealing with strongly nonlinear and multi-axial non-proportional stress/strain states, as demonstrated in (Berti et al., 2019). A set of constant life diagrams was built according to each criterion following the procedure detailed below:

- according to the boundary conditions in Table 1, each simulation was run to describe four complete fatigue cycles. This was aimed at guaranteeing the numerical stabilization of the local variables. These sets of boundary conditions were chosen to obtain different outputs for the fatigue criteria;
- the stress and strain tensors associated with different time instants of the last fatigue cycle were extracted from the centroids of those elements belonging to the stent functional unit (Figure 1, dashed box);
- an ad-hoc Matlab script (Matlab R2018a, MathWorks, Natick, MA) computed the values of the local variables according to each fatigue criterion;
- for each criterion, a constant-life chart was built with the specific FIs plotted against the first mean principal strain: each element value of FI appears as a dot in the plot;
- for each criterion, the experimental information regarding the material fatigue strength at 10^6 cycles was translated into a uniaxial limit curve: this was achieved by applying the same Matlab script to the stress and strain tensors of the FE uniaxial tests;
- the position of the FIs point cloud with respect to the material limit allowed the identification of either critical conditions (the points overcome the limit curve) or safe ones (the points are below the limit curve). A fatigue risk factor (RF), calculated as the difference between the FI and the limit curve at the same mean strain, was given for each element of the model in each configuration.

The outcome of each experimental test was evaluated together with the corresponding set of constant-life plots to identify which criterion was the most reliable in interpreting fatigue failure.

3. Results

3.1 Experimental tests and FE modeling

The mechanical tests allowed the identification of the Ni-Ti parameters: best fitting the experimental data with the FE curve (Figure 3 a), the parameters collected in Table 2 were obtained. The results of fatigue tests allowed to build the constant-life diagram reported in Figure 3b. The cases in which all the wires of each tested samples exhibited fracture before 10^6 cycles were interpolated to indicate the loading conditions leading to the failure of all samples (solid line in Figure 3b); similarly, an interpolation for the cases in which no wire fractured before 10^6 cycles was performed (dashed line in Figure 3b). Even if the limited number of tests does not allow us to associate a precise failure probability to the data acquired, the two lines allow making some considerations on the stent fatigue strength taking into account some experimental variability: with this aim in mind, in the following we have indicated the solid line as “failure limit curve” and the dotted line as “safe limit curve”.

From the experimental tests, both stent geometries reached the run-out in the P1 load case (2 tested specimens for each stent type). See Table 3 for details. When subjected to P2 load case, the three tested specimens for each type underwent fatigue failure at the same location: for the ABS stent, it happened at the intersection between the vertical link and the v-strut (see Figure 1 a, white arrow) while for the COMP stent in correspondence of the v-strut adjacent to the link (Figure 1 b, white arrow). The ABS stent fractured at about $2x10^5$ cycles (with maximum and minimum number of cycles of 246123 and 177311, respectively), while the COMP stent at about $2x10^4$ cycles (with maximum and minimum number of cycles of 22995 and 17012, respectively). The P3 load case led to run-outs for both the ABS and COMP specimens.

Table 2 Material parameters for the ABS_SUPER_ELASTIC material model in Abaqus 2018, calibrated from the experiments

Ni-Ti (ABQ_SUPER_ELASTIC material model)								
E_A (MPa)	E_M (MPa)	ν	ε_L	σ_{SAS} (MPa)	σ_{FAS} (MPa)	σ_{SSA} (MPa)	σ_{FSA} (MPa)	σ^C_{SAS} (MPa)
47000	22000	0.3	0.045	260	350	140	80	516

3.2 Multi-axial fatigue strength criteria

As for the numerical analysis, the effect of the stent design on the fatigue resistance can be understood at a glance from the distribution of the result point clouds (Figures 4, 5, 6). Fatigue prediction was affected by the choice of the multi-axial criterion, even if all of them agreed in the location of the most critical elements, which is in accordance with experimental observations (Figure 7). The VM index always expresses the highest RF (ABS: P1=1.79, P2=2.79, P3=1.94; COMP: P1=1.54, P2=3.40, P3=1.87) in all loading conditions, whilst a specific trend cannot be recognized for the other criteria (see Table 3).

The P1 represented the less detrimental set of boundary conditions (Figure 4): in both the stents, FS, BM and SWT point clouds lay below the failure limit curve (RF<1). As for ABS stent, only in the FS chart, the 1.1% of the points are in between the safe and failure limit curves; similarly, regarding the COMP stent, in the BM the 0.04% and in the FS the 4.1% are in between the safe and failure limit curves. When the P2 conditions were applied, all the criteria predict critical output leading to failure, with different RFs (Figure 5). In this case, the ABS stent exhibits a low fraction of critical elements (RFs>1), which is about 0.3% for the FS, BM and SWT, while the number increases according to the VM (2.1%). The COMP stent has a higher number of critical elements: the VM finds 21.9% of the point cloud above the failure limit curve, while the FS, BM and SWT lower this number to 7.0%, 4.9% and 4.0%, respectively. Finally, P3 is an intermediate case (Figure 6), where BM and SWT predict always a safe condition (RF<1, low element fraction in between the safe and failure limit curves. BM: 0.07%, SWT: 0.3%), while FS indicates a critical condition in the case of COMP stent (RF=1.17, 0.4% elements in between the safe and failure limit curve).

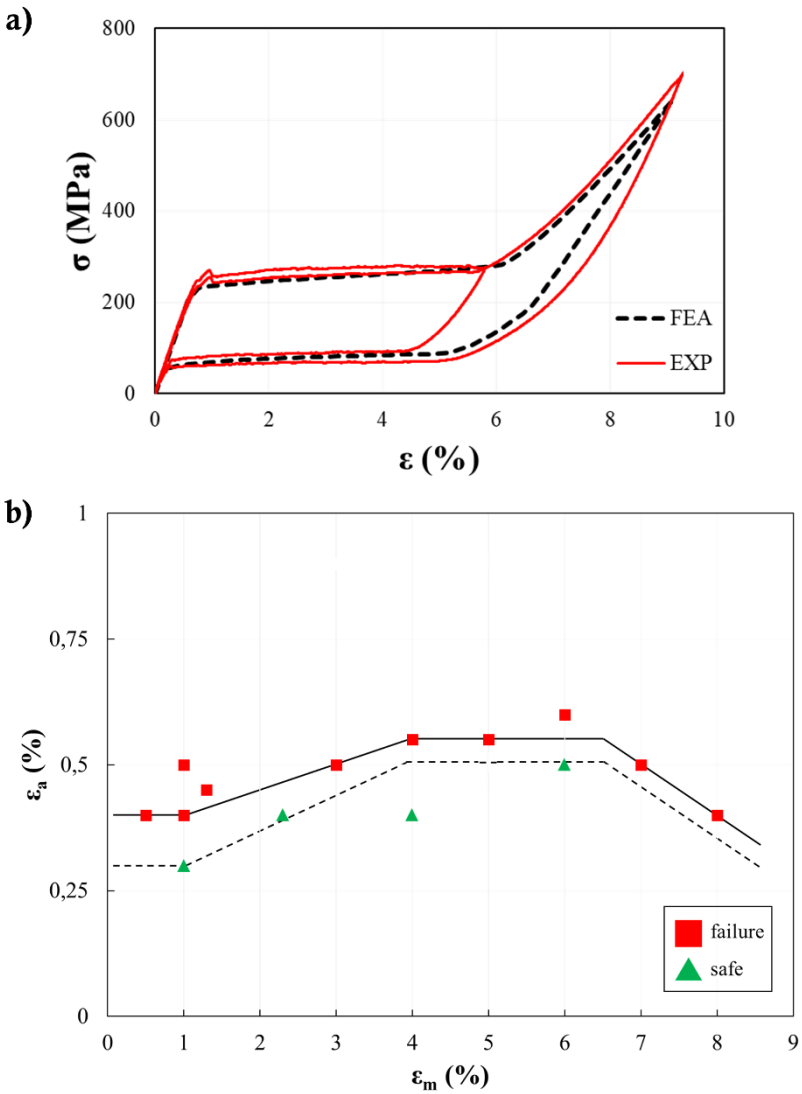

Figure 3 Ni-Ti material properties: a) comparison between the experimental loading-unloading tensile curve (solid line) and the corresponding FE result (dashed line) in terms of true stresses and strains; b) constant-life diagram obtained through uniaxial tensile fatigue tests at different values of mean strain and strain amplitude. The solid line is an interpolation of the loading conditions leading to the failure of all samples (failure limit curve); the dashed line is an interpolation of the loading conditions leading to no failure (safe limit curve).

Table 3 Maximum values for the numerical risk factors (RFs) for ABS and COMP stents under P1, P2 and P3 loads combinations and the corresponding experimental results

STENT ABS	FEA				EXP	
	Fatigue criteria				Output	# tests
Load case	VM	FS	BM	SWT		
P1	1.79	0.91	0.83	0.84	2 Run-out	2
P2	2.79	1.31	1.22	1.25	3 Failure	3
P3	1.94	0.97	0.86	0.90	3 Run-out	3
STENT COMP	FEA				EXP	
	Fatigue criteria				Output	# tests
Load case	VM	FS	BM	SWT		
P1	1.54	1.00	0.84	0.84	2 Run-out	2
P2	3.40	2.22	2.01	1.31	3 Failure	3
P3	1.87	1.17	1.00	0.85	2 Run-out	2

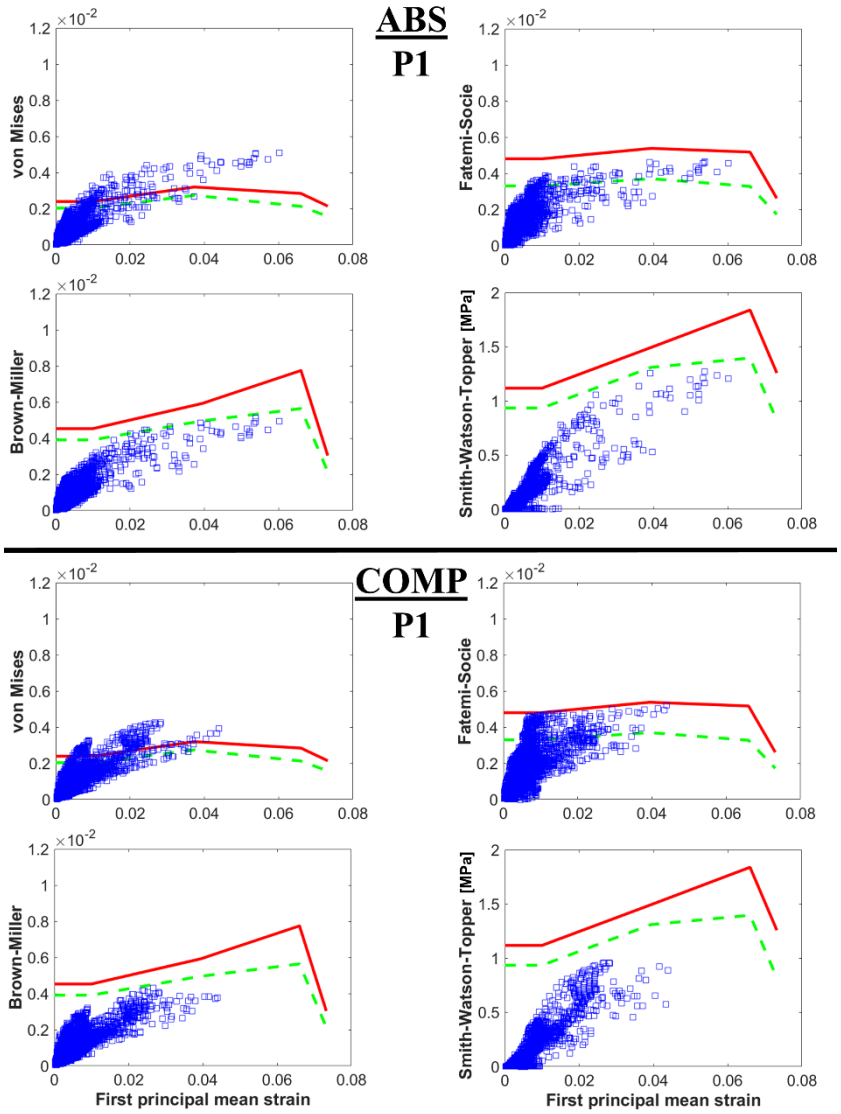

Figure 4 Results of different fatigue criteria under P1 condition: point clouds for ABS stent (top) and COMP stent (bottom) are compared with the failure and safe limit curves obtained interpolating the results of the fatigue tests on ad-hoc multi-wire specimens.

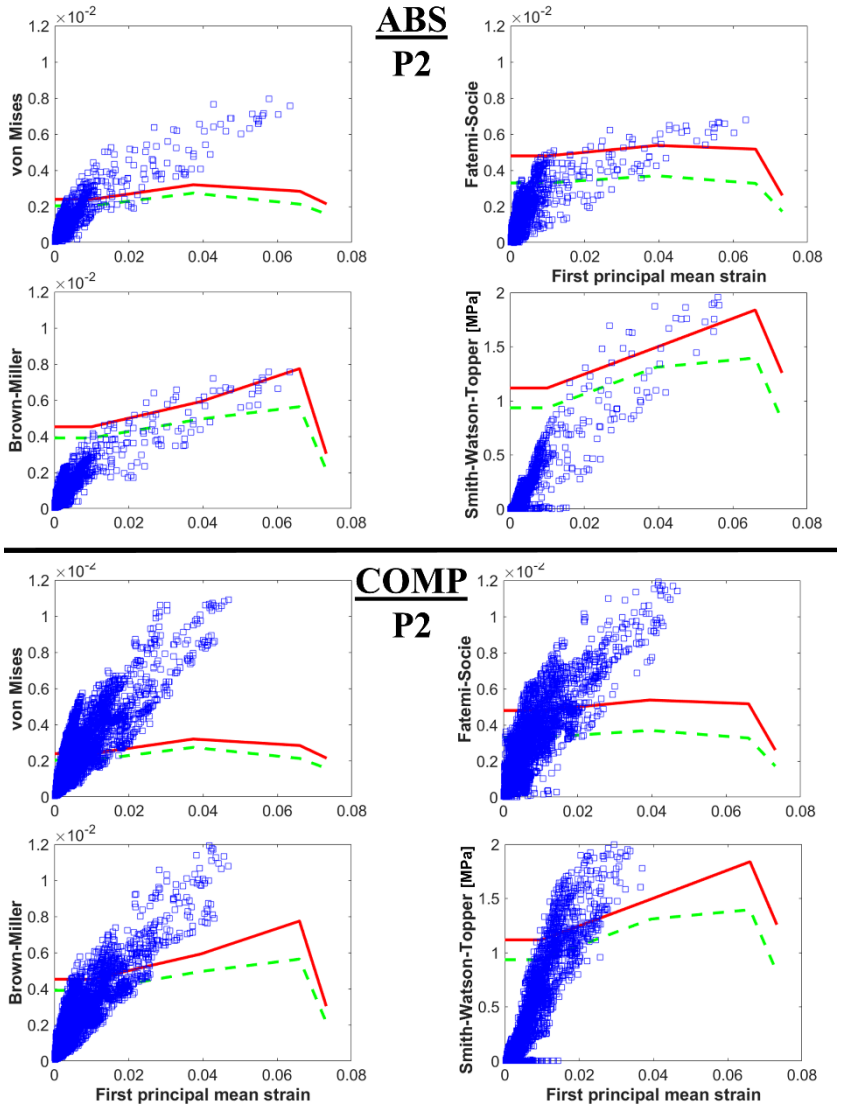

Figure 5 Results of different fatigue criteria under P2 condition: point clouds for ABS stent (top) and COMP stent (bottom) are compared with the failure and safe limit curves obtained interpolating the results of the fatigue tests on ad-hoc multi-wire specimens.

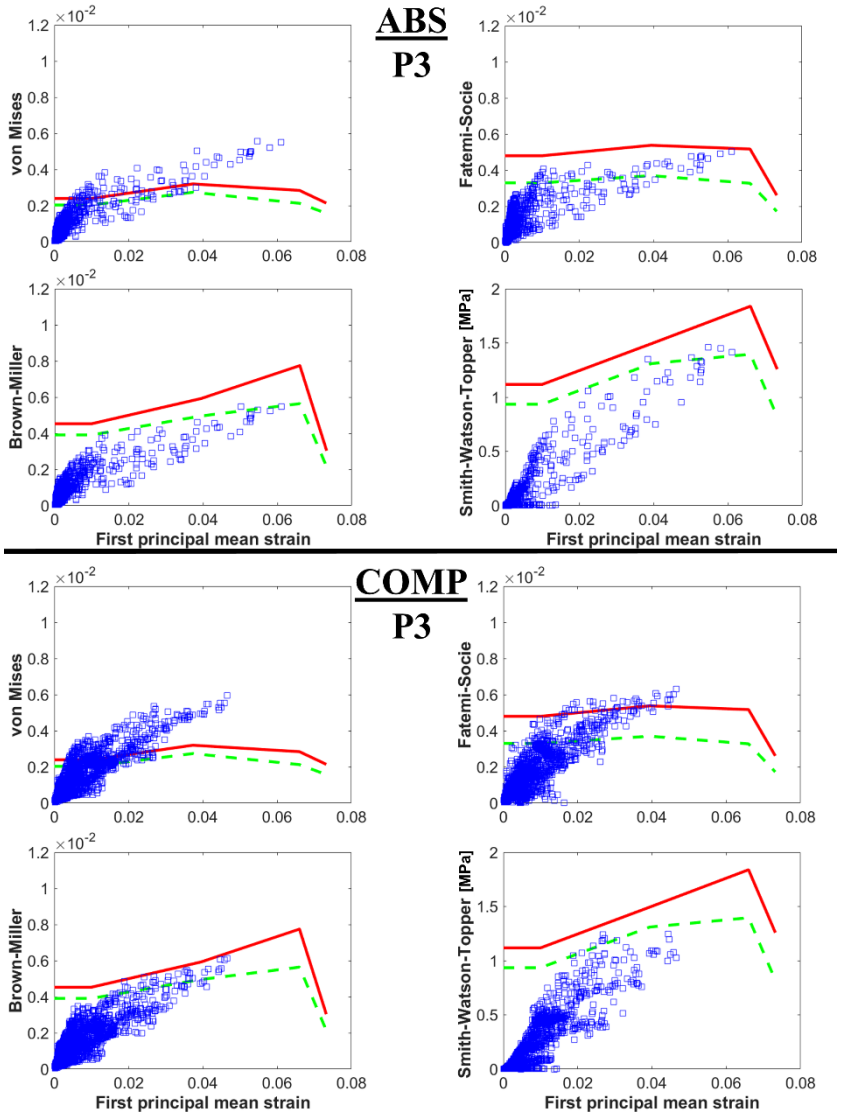

Figure 6 Results of different fatigue criteria under P3 condition: point clouds for ABS stent (top) and COMP stent (bottom) are compared with the failure and safe limit curves obtained interpolating the results of the fatigue tests on ad-hoc multi-wire specimens.

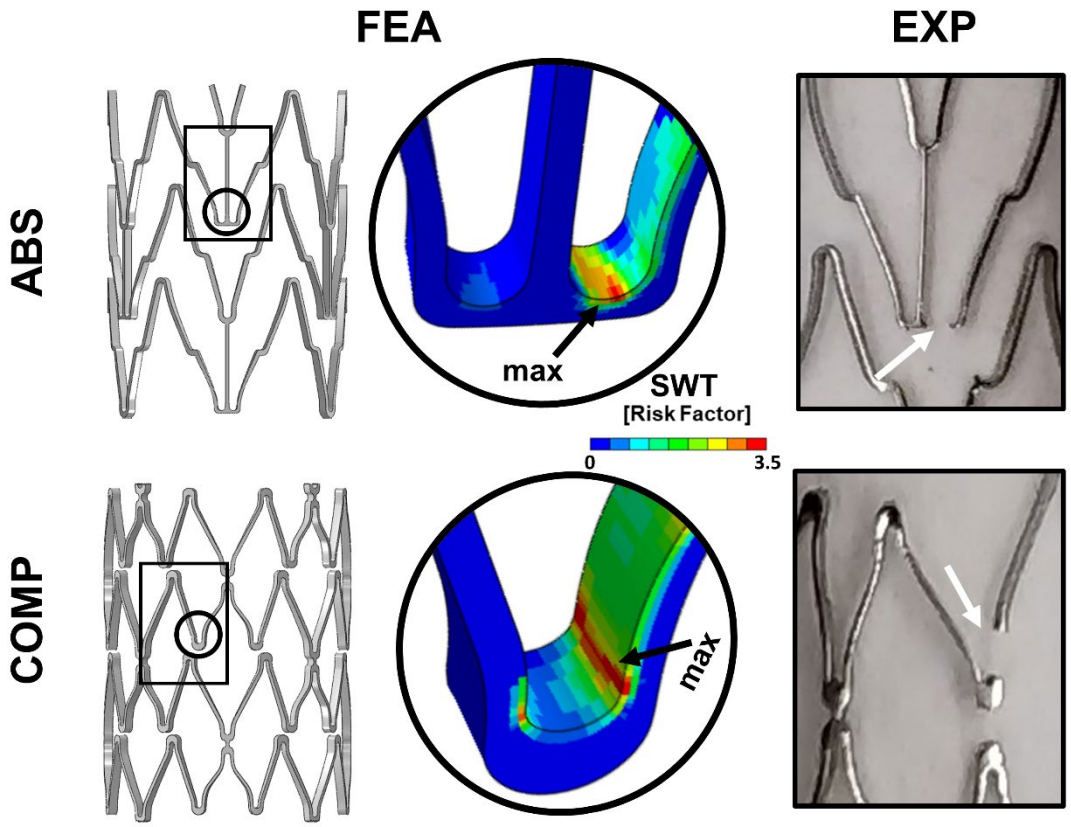

Figure 7 FE contour plots of the most critical area belonging to ABS stent and COMP stent, according to the SWT criterion under P2 load. All the criteria agreed in recognizing the same most critical area for the fatigue fracture for both the stent designs. The comparison with the experimental results showed a perfect match in the fracture location.

4. Discussion

The comparison between multi-axial fatigue experiments and numerical models allowed a better understanding of the fatigue behavior of peripheral Ni-Ti stents. For the loading conditions and stent types being considered, the standard approach for the Ni-Ti fatigue assessment, employing the equivalent Von Mises alternate strain as fatigue failure risk indicator (improperly, as already declared, herein defined as VM criterion), makes predictions in disagreement with experimental data in the case of P1 and P3 conditions. This allows us to argue that the use of VM criterion in Ni-Ti stent fatigue assessment might lead to conservative predictions. Therefore, VM criterion may be exploited to preliminary verify new prototypes with respect to fatigue-safe conditions, but it is not accurate when investigating the stent specific response under general cyclic loads.

The results indicate that the critical plane approaches, especially those of BM and SWT, are in greater concordance with the experimental data. This finding is supported by the results of previous numerical investigations, showing the local stress/strain response of the stents under cyclic multi-axial loads is always non-proportional even under proportional boundary conditions (Berti et al., 2019). Indeed, while the accuracy of VM is commonly limited to uniaxial or proportional loading conditions, critical plane criteria are suitable for non-proportional conditions.

It is interesting to note that BM and SWT criteria have a superior predictive capability in describing multi-axial fatigue strength of Ni-Ti peripheral stents, even if their fatigue indices were based on different mechanical assumptions on fatigue crack nucleations. BM recognizes the shear strain amplitude and normal strain amplitude are responsible for crack nucleation and propagation, respectively, while the SWT assumes fatigue life to be dominated by crack nucleation and growth along the plane of maximal principal strain. Both criteria share the presence of the normal strain amplitude ($\Delta\varepsilon_n$) in their formulation, which may be claimed as an important parameter in the description of Ni-Ti fatigue behavior. Clearly, any further consideration requires more experiments for increasing the reliability of the analysis; further non-proportional loads over a broader range of conditions should be investigated, in addition to deeper investigations at the microscale to define the mechanism governing crack nucleation and propagation.

The FS and BM FIs depend on the empirical constants k and S. In the absence of any suitable experimental data these were set to unity. Concern does arise that predictions will change if other values exist. Yet, the change in the position of the material fatigue limit and point clouds according to FS and BM criteria should drop as the constants fall and as such overall risk factor is not greatly affected and failure predictions do not change dramatically.

Comparing the distribution of the result point clouds of the two stents for the three load cases (Figures 4, 5, 6), it is worth noticing that, in the case of COMP stent, the FIs are always higher. In particular, for case P2 a higher number of points lays over the fatigue limit curve: this means a higher number of elements exhibiting risk of failure, which is compatible with the lower fatigue life of the experimental samples (one order of magnitude below the corresponding one of the ABS stent). Axial tensile tests performed (Allegretti et al., 2018) on both the stent types offer insight here. The ABS stent was more deformable than the COMP device due to the presence of fewer links between the rings (3 in the ABS, 4 in the COMP). Consequently, fewer ABS elements reach high deformation - 0.9% of the analyzed volume exceeds 2% mean strain compared to the 2.5% for the COMP stent. The material fatigue limit was assessed through uniaxial tensile tests on ad-hoc multi-wires samples to avoid issues deriving from the use of diamond-shaped specimens (Bonsignore, 2017). In fact, the use of FE models to calculate the internal state of stress and strain may be not trivial in such bending-dominated structures, whilst the mean and amplitude values of the strain can be easily obtained from the multi-wires specimens. Clearly, it would be also interesting to investigate the ratio between fatigue resistance in tension and in bending, considering that the stent struts are mainly subjected to bending during cyclic loads (Everett

et al., 2016). However, this investigation is not simple, considering that Ni-Ti properties are strongly affected by sample dimensions and thermomechanical exposure. Accordingly, it is of paramount importance to test the specific material (obtained applying the same processes adopted for the device) using ad hoc specimen size and shape, as performed in this paper. No approximations were introduced regarding the mechanical properties of the employed alloy, otherwise, the fatigue prediction capacity assessed by this combined experimental-numerical work might be affected by the features of the specific material fatigue limit curve.

Peripheral stents are usually required to survive 10^7 cycles, corresponding to 10 years of working conditions due to gait (Kinkel et al., 2009). Accelerated high-cycle fatigue tests are a common procedure (ASTM, 2013). The requirement to respect the physiological frequency of gait (about 1 Hz) over millions of cycles limited the possibility in this work of an extensive experimental campaign on the stents. For this reason, the run-out was reduced to 10^6 cycles, according to the available literature for Ni-Ti which recognizes almost constant fatigue properties between 10^5 and 10^7 cycles [5]. Clearly, the reduced number of tests performed for each load case makes the uncertainty on the fatigue strength associated with a given failure probability very large: a much wider experimental campaign must be performed for increasing the significance of the results.

5. Conclusions

In the present paper, the device response under multi-axial loads was investigated leveraging the knowledge of the static and fatigue properties of the specific material – herein the Ni-Ti shape memory alloy. The availability of ad-hoc multi-wires specimens enabled us to draw some conclusions about the device performance: no approximations were introduced regarding the employed alloy, which is rare in the available literature. Through a comparative study of multi-axial experimental tests and numerical simulations, critical plane criteria were demonstrated as reliable predictive tools in the fatigue assessment of Ni-Ti peripheral stents. These results imply that as stents are subject to in-vivo-like loads with a complex set of multi-axial boundary conditions more sophisticated criteria than the commonly used approach, based on the calculation of VM equivalent amplitude strain, are required to material fatigue especially if patient-specific conditions are to be considered. The VM approach can be exploited in the preliminary design and verification of new prototypes but is overly conservative in the complex domain of clinical use.

Due to the limited number of tested specimens, in the future, it will be necessary to run other tests, in order to perform a more reliable analysis of the results. Moreover, a generalization of these results requires an extension to more materials, loading conditions and fatigue criteria. Finally, it would be of paramount importance to know the Ni-Ti micro-mechanic response to cyclic loads, which is responsible for the crack nucleation and propagation. In this way, the choice of the proper fatigue criterion would be supported by the physics of this problem.

Acknowledgments

The authors acknowledge Medtronic-Invatec for the experimental samples produced in its laboratory, Mr. Dario Allegretti, PhD and Mr. Carlo Guala, MEng for their technical support provided within the project "RT3S-Real-Time Simulation for Safe Vascular Stenting" funded by the European Commission under the 7th Framework Programme, GS FP7-2009-ICT-4-248801 and Gurvan Jodin, PhD for assistance in designing the experimental set-up.

Elazer R Edelman is supported in part by a grant from the US National Institutes of Health (R01 49039). Francesca Berti and Francesco Migliavacca were partially supported by the Fondazione Fratelli Agostino and Enrico Rocca through a "Progetto Rocca" doctoral fellowship. Francesca Berti, Giancarlo Pennati, Francesco Migliavacca and Lorenza Petrini are partially funded by the H2020 Programme project InSilc "In-silico trials for drug-eluting BVS design, development and evaluation" (H2020-SC1-2017-CNECT-2-777119).

Bibliography

Allegretti, D., Berti, F., Migliavacca, F., Pennati, G., Petrini, L., 2018. Fatigue Assessment of Nickel–Titanium Peripheral Stents: Comparison of Multi-Axial Fatigue Models. Shape Mem. Superelasticity 4, 186–196. https://doi.org/10.1007/s40830-018-0150-7

Ansari, F., Pack, L.K., Brooks, S.S., Morrison, T.M., 2013. Design considerations for studies of the biomechanical environment of the femoropopliteal arteries. J. Vasc. Surg. 58, 804–813. https://doi.org/10.1016/j.jvs.2013.03.052

ASTM, 2013. F2477-19 Standard Test Methods for in vitro Pulsatile Durability Testing of Vascular Stents. https://doi.org/10.1520/F2477-07.proper

ASTM F 2516-18, 2018. Standard Test Method for Tension Testing of Nickel-Titanium Superelastic Materials.

Berti, F., Spagnoli, A., Petrini, L., 2019. A numerical investigation on multiaxial fatigue assessment of Nitinol peripheral endovascular devices with emphasis on load non-proportionality effects. Eng. Fract. Mech. 216, 106512. https://doi.org/10.1016/j.engfracmech.2019.106512

Bonsignore, C., 2017. Present and future approaches to lifetime prediction of superelastic nitinol. Theor. Appl. Fract. Mech. 92, 298–305. https://doi.org/10.1016/j.tafmec.2017.04.001

Brown, M.W., Miller, K.J., 1973. A Theory for Fatigue Failure under Multiaxial Stress-Strain Conditions. Proc. Inst. Mech. Eng. 187.

Dordoni, E., Petrini, L., Wu, W., Migliavacca, F., Dubini, G., Pennati, G., 2015. Computational Modeling to Predict Fatigue Behavior of NiTi Stents: What Do We Need? J. Funct. Biomater. 6, 299–317. https://doi.org/10.3390/jfb6020299

Duerig, T., Pelton, A., Stöckel, D., 1999. An overview of nitinol medical applications. Mater. Sci. Eng. 273–275, 149–160. https://doi.org/10.1016/S0921-5093(99)00294-4

Everett, K.D., Conway, C., Desany, G.J., Baker, B.L., Choi, G., Taylor, C.A., Edelman, E.R., 2016. Structural Mechanics Predictions Relating to Clinical Coronary Stent Fracture in a 5 Year Period in FDA MAUDE Database. Ann. Biomed. Eng. 44, 391–403. https://doi.org/10.1007/s10439-015-1476-3

Fatemi, A., Socie, D.F., 1988. A critical plane approach to multiaxial fatigue damage including out-of-phase loading. Fatigue Fract. Eng. Mater. Struct. 11, 149–165.

Gates, N.R., Fatemi, A., 2016. Interaction of shear and normal stresses in multiaxial fatigue damage analysis. Frat. ed Integrita Strutt. 10, 160–165. https://doi.org/10.3221/IGF-ESIS.37.22

Kinkel, S., Wollmerstedt, N., Kleinhans, J.A., Hendrich, C., Heisel, C., 2009. Patient activity after total hip arthroplasty declines with advancing age. Clin. Orthop. 467, 2053–2058. https://doi.org/10.1007/s11999-009-0756-3

MacTaggart, J.N., Phillips, N.Y., Lomneth, C.S., Pipinos, I.I., Bowen, R., Timothy Baxter, B., Johanning, J., Matthew Longo, G., Desyatova, A.S., Moulton, M.J., Dzenis, Y.A., Kamenskiy, A. V., 2014. Three-dimensional bending, torsion and axial compression of the femoropopliteal artery during limb flexion. J. Biomech. 47, 2249–2256. https://doi.org/10.1016/j.jbiomech.2014.04.053

Mahtabi, M.J., Shamsaei, N., 2015. Multiaxial fatigue modeling for Nitinol shape memory alloys under in-phase loading. J. Mech. Behav. Biomed. Mater. 55, 236–249. https://doi.org/10.1016/j.jmbbm.2015.10.022

Maletta, C., Sgambitterra, E., Niccoli, F., 2016. Temperature dependent fracture properties of shape memory alloys: Novel findings and a comprehensive model. Sci. Rep. 6, 1–11. https://doi.org/10.1038/s41598-016-0024-1

Morrison, T.M., 2016. Reporting of Computational Modeling Studies in Medical Device Submissions - Draft Guidance for Industry and Food and Drug Administration Staff. https://doi.org/https://bit.ly/36rYMUw

Pelton, A.R., Schroeder, V., Mitchell, M.R., Gong, X.Y., Barney, M., Robertson, S.W., 2008. Fatigue and durability of Nitinol stents. J. Mech. Behav. Biomed. Mater. 1, 153–164. https://doi.org/10.1016/j.jmbbm.2007.08.001

Petrini, L., Migliavacca, F., 2011. Biomedical Applications of Shape Memory Alloys. J. Metall. 2011, 1–15. https://doi.org/10.1155/2011/501483

Petrini, L., Trotta, A., Dordoni, E., Migliavacca, F., Dubini, G., Lawford, P. V., Gosai, J.N., Ryan, D.M., Testi, D., Pennati, G., 2016. A Computational Approach for the Prediction of Fatigue Behaviour in Peripheral Stents: Application to a Clinical Case. Ann. Biomed. Eng. 44, 536–547. https://doi.org/10.1007/s10439-015-1472-7

Robertson, S.W., Pelton, A.R., Ritchie, R.O., 2012. Mechanical fatigue and fracture of Nitinol. Int. Mater.

Rev. 57, 1–37. https://doi.org/10.1179/1743280411Y.0000000009
Runciman, A., Xu, D., Pelton, A.R., Ritchie, R.O., 2011. An equivalent strain/Coffin-Manson approach to multiaxial fatigue and life prediction in superelastic Nitinol medical devices. Biomaterials 32, 4987–4993. https://doi.org/10.1016/j.biomaterials.2011.03.057
Scalet, G., Conti, M., Auricchio, F., 2017. Computational Analysis of Advanced Shape-Memory Alloy Devices Through a Robust Modeling Framework. Shape Mem. Superelasticity 3, 109–123. https://doi.org/10.1007/s40830-017-0102-7
Shahriar, S., Fatemi, A., 2019. On the interaction of normal and shear stress in multiaxial fatigue damage. Fatigue Fract. Eng. Mater. Struct. 1–17. https://doi.org/10.1111/ffe.13070
Shamsaei, N., Fatemi, A., 2009. Effect of hardness on multiaxial fatigue behaviour and some simple approximations for steels. Fatigue Fract. Eng. Mater. Struct. 32, 631–646. https://doi.org/10.1111/j.1460-2695.2009.01369.x
Smith, K.N., Topper, T.H., Watson, P., 1970. A stress–strain function for the fatigue of metals (stress-strain function for metal fatigue including mean stress effect). J Mater. 5, 767–778. https://doi.org/10.1179/1752270612Y.0000000008
Socie, D., 1987. Multiaxial Fatigue Damage Models. J. Eng. Mater. Technol. 109, 293. https://doi.org/10.1115/1.3225980
Socie, D.F., Waill, L.A., Dittmer, D.F., 1985. Biaxial fatigue of Inconel 718 including mean stress effects. Multiaxial Fatigue 463–481. https://doi.org/https://doi.org/10.1520/STP36238S
Suresh, S., 1998. Fatigue of Materials. Cambridge University Press. https://doi.org/10.1017/CBO978511806575
Susmel, L., 2009. Multiaxial notch fatigue. Woodhead Publishing Limited.